Measurement of surface shear stress vector distribution using shear-sensitive liquid crystal coatings

Article *in* Acta Mechanica Sinica · October 2012

DOI: 10.1007/s10409-012-0144-1

CITATIONS
7

READS
290

3 authors, including:

Jisong Zhao
Nanjing University of Aeronautics & Astronautics
16 PUBLICATIONS **60** CITATIONS

SEE PROFILE

Peter Scholz
Technische Universität Braunschweig
60 PUBLICATIONS **353** CITATIONS

SEE PROFILE

Acta Mechanica Sinica (2012) 28(5):1261–1270
DOI 10.1007/s10409-012-0144-1

RESEARCH PAPER

Measurement of surface shear stress vector distribution using shear-sensitive liquid crystal coatings

Ji-Song Zhao · Peter Scholz · Liang-Xian Gu

Received: 18 November 2011 / Revised: 22 March 2011 / Accepted: 11 June 2012

Abstract The global wall shear stress measurement technique using shear-sensitive liquid crystal (SSLC) is extended to wind tunnel measurements. Simple and common everyday equipment is used in the measurement; in particular a tungsten-halogen light bulb provides illumination and a saturation of SSLC coating color change with time is found. Spatial wall shear stress distributions of several typical flows are obtained using this technique, including wall-jet flow, vortex flow generated by a delta wing and junction flow behind a thin cylinder, although the magnitudes are not fully calibrated. The results demonstrate that SSLC technique can be extended to wind tunnel measurements with no complicated facilities used.

Keywords Shear-sensitive liquid crystal (SSLC) · Surface shear stress measurement · Wall-jet · Vortex generator · Junction flow

1 Introduction

Wall shear stress is an important fluid-mechanic parameter. In aerodynamics research, much valuable information can be gained from visualizing and measuring shear stress patterns on solid surfaces. Frictional forces generated by gases or liquids flowing over these surfaces can significantly influence the performance of aircraft, ships, or surface-transport vehicles. Internal frictional forces, such as those caused by air compression through a jet engine or blood flow through an artificial heart chamber, also affect aerodynamic or mechanical performance.

J.-S. Zhao (✉) · L.-X. Gu
School of Astronautics, Northwestern Polytechnical University, 710072 Xi'an, China
e-mail: zhaojisongjinling@163.com
J.-S. Zhao · Peter Scholz
Institute of Fluid Mechanics, TU Braunschweig, 38106 Braunschweig, Germany

Wall shear stress measurements remain very challenging. In the past, various mechanical or electrical means has been developed for wall shear stress measurement, such as mechanical balances or intrusive probes and sensors [1, 2]. However, these methods typically disturbed the flow and measured point-wise. Any means to measure shear stress efficiently with a high spatial resolution would be interesting.

Shear-sensitive liquid crystal (SSLC) technique is a global wall shear stress measurement technique and was first explored by Reda et al. [3–5] of NASA Ames Research Center. The observables from SSLC are transient color changes that result from the change in the pitch of the helix of the cholesteric structure of SSLC due to change in mechanical stress. The color is known to vary with the shear stress direction and magnitude and the angles of observation and illumination. When the color is calibrated against such parameters, the visualized color image can be converted into a shear stress field. SSLC technique has been used in several measurements including shear stress fields in the flow beneath a tangential wall jet [4] and an oblique impinging jet [5], shear stress fields over flat surface around a cylinder in steady [6] and instantaneous flows [7], and shear stress field over curved surface (NACA0018 airfoil) [8].

Surface stress-sensitive film (S^3F) is a recently developed global wall shear stress measurement technique, which utilizes PIV-like correlation technique and fluorescence to measure the deformation field of a specifically designed polymeric film under the action of wall shear stress [9, 10]. The polymeric film is doped with luminescent molecules and seeded with tracer particles. Shear stress and pressure are simultaneously extracted from the tangential and normal components of deformation based on a system model since S^3F is sensitive to both of them. The capability of S^3F has been demonstrated in several flows in small facilities to measure the topological structures of wall shear stress fields.

Global skin friction diagnostics based on surface luminescent oil [11, 12] and temperature visualizations [13] have also been developed recently. The former is based on the

relationship between the skin friction and the luminescent intensity of an oil film doped with luminescent molecules. Skin friction field can be determined by solving the Euler–Lagrange equations. The technique has been used in various complex separated flows [11, 12]. Similarly, the latter utilizes the asymptotic form of the energy equation near a wall to provide a relation between the skin friction vector, heat flux and temperature at a wall, and a relative skin friction field can be extracted from surface temperature images by solving the Euler–Lagrange equations as an inverse problem. The skin friction distributions on a flat surface in the normal and oblique impinging jets were extracted by using this method [13].

Although impressive shear stress distributions have been obtained using the aforementioned global wall shear stress measurement techniques, none of them has been used as a routine, quantitative technique for wind-tunnel testing and other practical measurements. The present paper mainly focuses on SSLC technique in wind tunnel measurement. As a global technique, SSLC is capable of measuring surface shear stress distribution over an entire surface in a continuous, non-intrusive manner. The main advantage of SSLC technique is that the responses of SSLC to wall shear stress are colorful and visible with a high resolution both in space and in time, thus can immediately reveal cause-and-effect relationships between changes in model configuration or test condition and the resulting surface shear stress field. In fact, SSLC has been used extensively in flow visualization recently [14–16]. One disadvantage of SSLC technique is the sensitivity to illumination and observation angles, which has been a barrier to its use for quantitative on complicated models, especially on curved surface. However, efforts have been made to extend SSLC technique to measure wall shear stress over curved surface [7]. Another disadvantage of SSLC technique is the need for optical access from certain positions to acquire data, which is not accessible in many wind tunnels. To overcome this difficulty, Reda et al. [17] has explored application of SSLC flow visualization through a transparent test surface.

The research of Reda et al. and Fujisawa et al. were conducted in carefully-arranged conditions. There are some problems in extending the measurement techniques to wind tunnel studies. In Reda et al.'s research, a special illumination source (NAC Visual Systems HMI-1200) was used to supply normal white light. This lighting is not easily accessible to other researchers. Moreover, a new SSLC coating was applied for each view, making measurements complicated and expensive. In the research of Fujisawa et al. [18], the calibration methodology required rotation of the test section, which made the calibration facility rather complicated. In our early researches, SSLC technique was extended for using in wind tunnel-like conditions. The purpose of the present paper is to further extend SSLC technique to wind tunnel measurements, with all special facilities replaced by common ones. Wall shear stress distributions in several typical flows, including wall-jet flow, vortex flow generated by a delta wing and junction-flow behind a thin cylinder, have been measured using SSLC technique, although not fully calibrated.

2 Experimental apparatus

2.1 General description

The experiments were conducted on the test plate of a low-speed wind tunnel at the Institute of Fluid Mechanics at TU Braunschweig, Braunschweig, Germany. The maximum velocity within the wind tunnel is 27.4 m/s. The tunnel has a test plate of 758 mm by 420 mm with an oblate elliptical leading edge. To enhance the quality of the color change in SSLC, a black anodized aluminum plug of 100 mm by 100 mm was mounted in the center of the test plate. The test plate was used to define the physical x-y plane, and the flat plate centerline (also the plug centerline) was used to define the $\phi = 0°$ reference. A rotating arm was built so that the above-plane view angle (denoted as α) was constant when recording the coating color change at different circumferential view angles (also called in-plane view angle and denoted as ϕ). Figure 1 shows the photograph and schematic diagram of experimental set-up. The arm can be rotated from $\phi = -90°$ to $\phi = 90°$ so that it is able to measure shear stress where no reverse flow exists. To measure reverse flow, a new set-up must be designed so that optical access is available between $\phi = -180°$ and $\phi = 180°$.

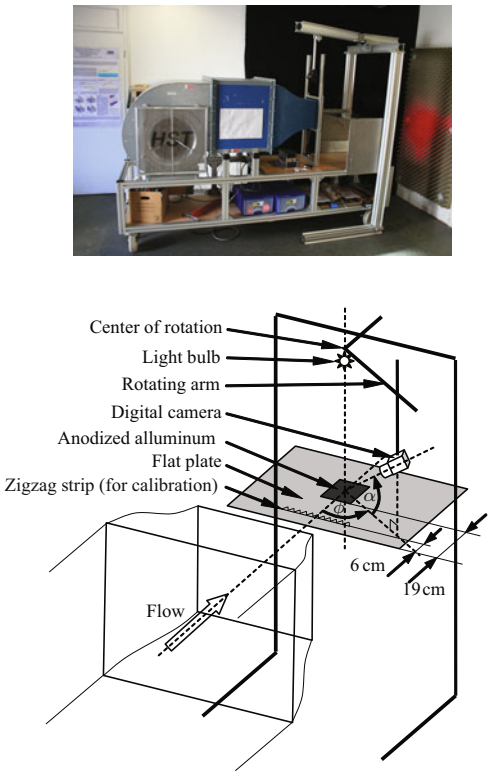

Fig. 1 Photograph and schematic diagram of the experimental set-up

2.2 Setting of above-plane view angle

The camera above-plane view angle was set to a constant with the help of the rotating arm. However, the angle should be optimized to maximize the color change in SSLC. A comparison of color change at different above-plane view angles is given in Fig. 2. The comparison experiment was conducted on the flat plate at a wind-tunnel outlet velocity of 23.0 m/s. The hue of each view is the average value across an area of 6 cm by 6 cm. It is clear that SSLC is more sensitive at a smaller above-plane view angle. However, the angle should not be set too small in this research otherwise the camera would be blocked by the top of the wind tunnel mouth. Very small above-plane view angle would also induce considerable image calibration error. In the following experiments, the above-plane view angle was set at about 28°.

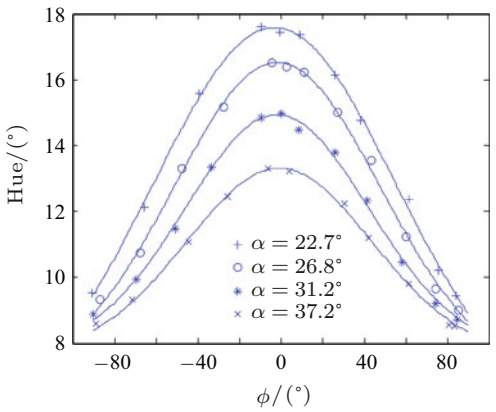

Fig. 2 Hue-ϕ curve at different above-plane view angles (u = 23.0 m/s)

2.3 Illumination source

In extending the Reda et al.'s research to wind tunnel measurements, the biggest difficulty was the special lighting needed to supply parallel normal white light. Unfortunately, such a light source is complicated and currently not commercially available. In our experimental set-up, we looked for a simple light source as a substitute. A wind tunnel experiment was designed to verify whether the light source was suitable in measurements. As illustrated in Fig. 3, the light source was placed at a height of 86 cm above the center of a flat plate, illuminating an area of interest of size 6 cm by 6 cm. The experiment was conducted at a wind tunnel velocity of 19.9 m/s. The flow was generally the same across the square and so the hue-ϕ curve at the center, left, up, right, and down (viewing downstream) of the square should coincide with each other if the light directions were sufficiently parallel.

A number of different light sources were tested in our preliminary study. It was found that extended light was better than focused light because the latter always had some halation. However, none of these provided suitable lighting for SSLC technique. Typical hue-ϕ curves at the five locations are given in Fig. 4, which were obtained under the illumination of a 40 W incandescent lamp with a lampshade diameter of about 15 cm. The hue was the average value of a window of size of 1 cm by 1 cm at each location. The curves do not coincide with each other due to perspective differences. It is easy to compute that the illumination angle varies about 14° among the five locations. Taking into consideration Figs. 3 and 4, we conclude that oblique illumination causes the hue-ϕ curve to shift towards the direction of light and become a little symmetrical about the light plane, in agreement with Reda et al. [19].

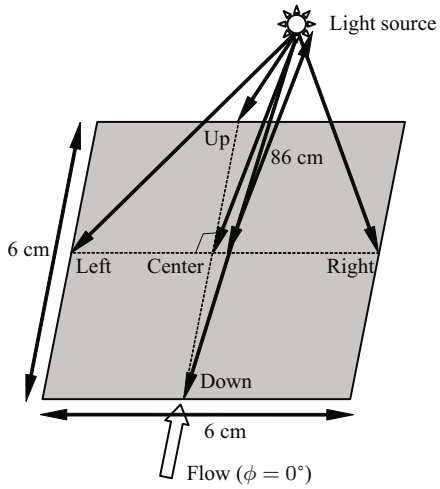

Fig. 3 Illumination angle differences across the five locations

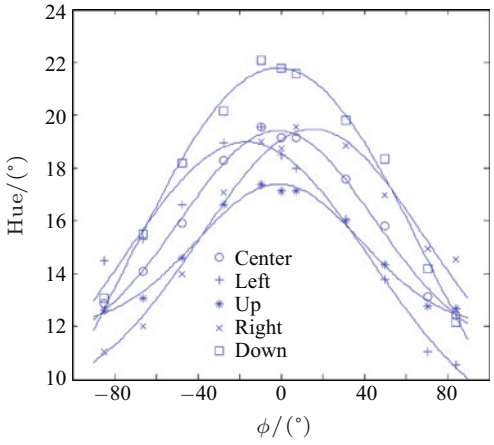

Fig. 4 Hue-ϕ curves at the five locations (u = 19.9 m/s, incandescent lamp illumination)

Because none of the many lights we tested were suitable, we decided to build a light source ourselves. We constructed a 20 W small tungsten halogen bulb with a thin aluminum shielding cap attached to the top to reduce the reflection of the ceiling and experimental shelves. The maximal size of the bulb was about 5 mm, so the angle differences of the light to each of the five locations was less than 4.3°. This difference could be further reduced by increasing the height

of the bulb above the plate. Figure 5 gives the hue-ϕ curves at the same five locations under the illumination of our light bulb. The five curves coincide well with each other. The maximum hue of each curve varies from 13.7° to 14.9° and the symmetry angle varies from −2.9° to 3.1°. The slight discrepancies were mainly due to uneven coating thickness. One drawback of this self-made light source was its low intensity. Exposure times were about 1 s, even when the lens aperture was set to the maximum value, and therefore did not enable instantaneous flow measurements to be taken.

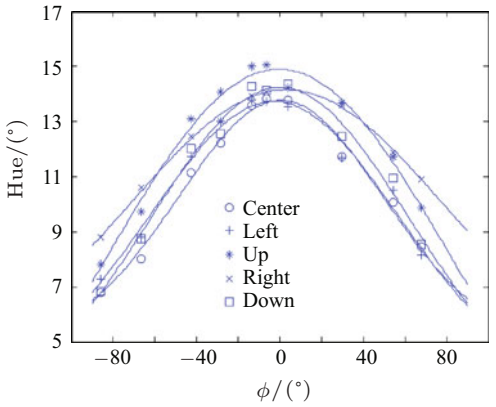

Fig. 5 Hue-ϕ curves at the five locations (u = 19.9 m/s, illuminated with a small light bulb)

2.4 Image facility and color calibration

A frame grabber and video camera was used in the work of Reda et al., and the color was calibrated with the standard Macbeth color checker. In this investigation, images were recorded with a Canon EOS 400D color digital camera (made in China). The "Manual" shot mode was used with the lens aperture set to F = 5.6 and the exposure time set to T = 1 s. A page of white A4 printing paper was used to set the customized white balance. There is no need to calibrate the color in standard color space, thus a self-made Macbeth color checker which was generated on a computer and printed on high quality color printer was used to calibrate the color [20]. The color calibration was found to be helpful in reducing random noises and was performed any time the imaging system (illumination source or digital camera) was changed to standardize color measurements in an even space.

2.5 Liquid crystal coating application technique

The SSLC mixtures used in this investigation were supplied by LCR Hallcrest (U.K.). Two mixtures (BCN/192 and BN/R50C) were analyzed as part of the present research. The liquid crystals were uniformly sprayed onto the aluminum "plug" with an air brush after being mixed with acetone (about 10% SSLC in volume). The acetone evaporated quickly after spraying, leaving a red SSLC coating on the test surface. The coating should be in the Grandjean texture because of its red color. The thickness of the coating is about 10 μm (based on mass conservation and estimated spray losses). It was found that an SSLC coating that is too thin gave little color change whereas one too thick tended to flow.

3 Saturation of SSLC coating color change

The most widely used liquid crystals in shear stress measurement are cholesteric (or chiral nematic) liquid crystals. Cholesterics can form textures of two types which are of primary interest in applications: the focal-conic texture and the Grandjean (or planar) texture [1]. The focal-conic texture does not reflect light selectively and, therefore, looks colorless. Under a shear stress, the focal-conic texture transforms into the planar texture. This textural transition is accompanied by emergence of a selectively reflected light, and the cholesteric sample takes on color. Thus there have been two primary implementations of shear sensitive liquid crystal coating techniques. One involves the color change associated with a shear induced texture change from focal-conic to Grandjean. The other involves the application of the selective reflection properties when SSLC coating is aligned in the Grandjean texture. Bonnet et al. [21] observed that the focal conic texture persisted until the combination of shear level and test time was sufficient to align the liquid crystals and to change the coating texture to Grandjean. Mee et al. [22] used this texture change to locate transition and obtain quantitative information in transitional boundary layer flows.

The current research focuses on the steady state color a Grandjean texture liquid crystal coating exhibits when shear-stress acts on it. In an early research, Reda et al. [19] declared that the response time of a Grandjean texture liquid crystal coating was of the order of millisecond and a coating was generally repeatable for measurements. But in all of their later published researches, Reda et al. [4, 5, 23] addressed a new coating which was applied for each view without any explanations. In our research, it is found that a Grandjean texture liquid crystal coating takes some time to give a steady color change. An experiment was designed to quantity the time dependent of the color change of SSLC coating. The experiment was conducted at a wind tunnel outlet velocity of 27.4 m/s. A screw cap was applied onto the anodized aluminum "plug" to increase the surface shear stress. Four raw images are given in Fig. 6 to illustrate the coating color change at different times (The wind tunnel was turned on at t = 14 s). The resolution was set so that 1 mm in physical coordinate corresponds to 5 pixels in image plane. The hue values varying with time at four locations along the jet centerline (u = 100; v = 1, 100, 200, and 300 respectively in the image plane in Fig. 6) are plotted in Fig. 7. The hue values increase monotonically at the beginning, but approach saturations at about t = 100 s at the four tested shear stress levels. Since there is a saturation of the color change, the same coating can be used for all the views required for the Gauss curve fit. Further experiments are all conducted more than 100 s after the tunnel is turned on.

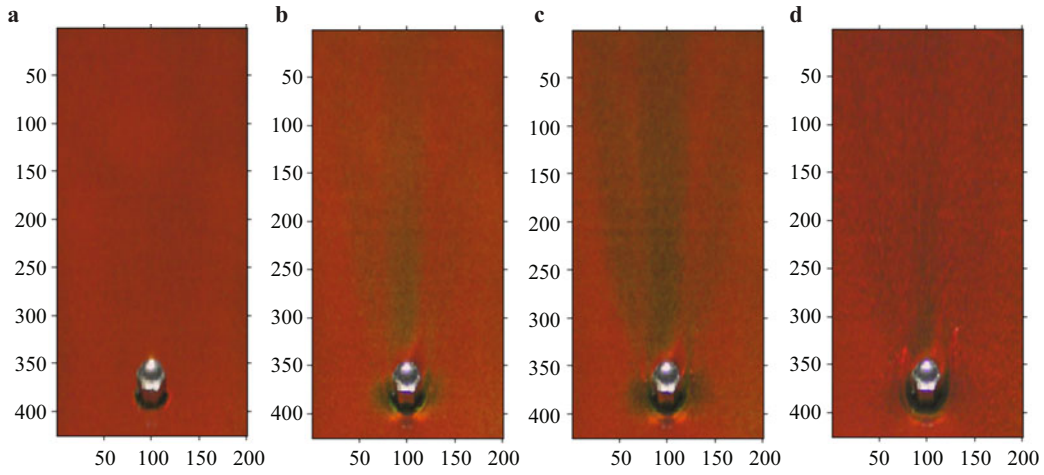

Fig. 6 Coating color change varied with time (brightness and contrast artificially increased by 20% for printing purposes). **a** $t = 0$ s; **b** $t = 53$ s; **c** $t = 138$ s; **d** Turn off the tunnel

Some important conclusions can be drawn from these findings. There is some dependence between the saturation and the shear stress: If the shear stress is larger (e.g., position $u = 100$, $v = 300$), the color saturates earlier. The color change is reversible. Once the force is removed, the coating renders the original dark red, as given in Fig. 7d. There is some deformation of the coating in Fig. 7d, which is because the coating was blew in a quite time (more than 450 s), and the coating was also a little too thick. When the tunnel was turned on again, the color change went to saturation immediately, and no time saturation was observed. Thus it can be seen the original coating went to the rapid color play state with the help of shear stress. It seems that the original coating was a mixture textures of focal-conic and Grandjean, and went into fully Grandjean texture under the shear, although it looks red. Further research is required on this topic.

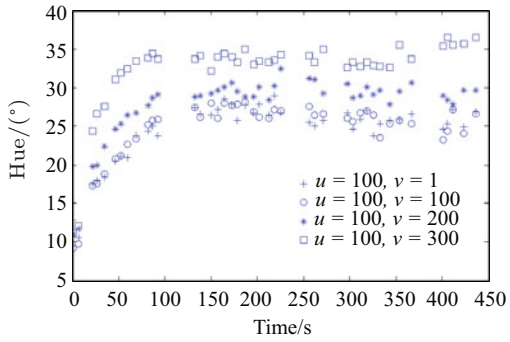

Fig. 7 Hue values variation with time at 4 chosen locations

4 Transformation of color image to shear stress distribution

To analyze the color change in SSLC coatings in physical coordinates, we performed a perspective transformation on each image to map the image coordinates to the physical coordinates on the test surface. Exterior parameters for the camera were determined for each image using four reference marks that were machined at the vertices of the square around the "plug".

For color measurements, it is more useful to represent the signal in terms of hue, saturation, and intensity (HSI) rather than red, green, and blue (RGB). Only the hue images were used for further analysis. Spatial filters over the 10×10 pixels neighborhood were applied to all the hue images to reduce the standard deviation of the hue variation while preserving the hue gradient. According to the second trichromic system discussed in Ref. [24], the hue can be calculate from

$$h = \tan^{-1}\frac{\sqrt{3}(G-B)}{2R-G-B} + \theta,$$
$$\theta = \begin{cases} 0, & 2R \geqslant G+B, \\ \pi & 2R < G+B, \end{cases} \tag{1}$$

where h is the hue, $h \in [-90°, 270°)$; R, G, and B are the three primary colors, red, green and blue, respectively. In this trichromic system, red ($R = 1$, $G = 0$, $B = 0$) is placed at 0°, green ($R = 0$, $G = 1$, $B = 0$) is placed at 120°, and blue ($R = 0$, $G = 0$, $B = 1$) is placed at 240°.

Reda et al. [25] found that, under normal illumination and fixed above-plane viewing angle, the maximum hue of SSLC coating for a given shear stress magnitude was measured when the shear vector was aligned with, and directed away from, the observer; changes in circumferential angle either side of the vector aligned position resulted in symmetric decrease in hue. The hue-ϕ change could be well fit by a Gaussian curve between −90° and 90°,

$$h(\phi) = (h(\phi_\tau) - h_{\mathrm{VN}}) \cdot \exp\left[-\left(\frac{\phi-\phi_\tau}{\sigma}\right)^2\right] + h_{\mathrm{VN}}, \tag{2}$$

where h_{VN} is the hue observed for an in-plane view angle normal to the shear vector (i.e., $|\phi_\tau - \phi| = 90°$), σ is the

standard deviation of the Gaussian distribution, ϕ_τ and $h(\phi_\tau)$ are the orientation of the shear stress vector and the hue observed when ϕ is aligned with the vector (referred to as vector-aligned hue), respectively.

A calibration curve of vector-aligned hue vs. shear stress magnitude is required for the specific arrangement wherein the calibration shear stress vector is aligned with and directed away from the camera. In Reda et al.'s research, fringe-imaging (oil-drop) skin friction technique was used for this purpose. In our research, the friction formula over a flat plate was used to calibrate the vector-aligned hue vs. shear stress magnitude. A zigzag strip was applied 6 cm away from the flat plate leading edge to trip the boundary layer. The measurement was made at the center of the anodized aluminum (18 cm downstream of the strip, see the schematic diagram in Fig. 1). The boundary layer was supposed to be a fully developed turbulent boundary layer and a reasonable local turbulent friction over the flat plate is

$$\tau = \frac{1}{2}\rho u^2 c_\mathrm{f},\ c_\mathrm{f} = 0.059\,2Re^{-1/5},\ Re = \frac{\rho u l}{\mu}, \tag{3}$$

where ρ is the air density, u is the wind tunnel outlet velocity, l is the reference length, measured from the leading edge of the test plate, μ is the dynamic viscosity, and Re is the Reynolds number. However, the development of boundary layer is very complicated and impacted by many factors. If the boundary layer is not fully turbulent, Eq. (3) is not correct or at least not accurate. In further research, the velocity profile should be measured to verify whether the boundary layer is a fully-developed turbulent boundary layer.

The camera in-plane view angle $\phi = 0°$ served as the angular reference point. The wind tunnel outlet velocity could be varied, as did the shear stress magnitude. The vector-aligned hue vs. shear stress magnitude calibration curves for two shear sensitive SSLC mixtures (BN/R50C and BCN192) are shown in Fig. 8. Note that BN/R50C is well calibrated while BCN192 is only partially calibrated. This is because BCN192 has a viscosity four times of that of BN/R50C, the maximum outlet velocity (27.4 m/s) was not high enough to generate sufficient friction, as displayed in Fig. 8. Unfortunately, BN/R50C was found not fit for surface shear stress measurement because of its too low viscosity in our early research [18]. Further measurements in the present paper were all conducted using BCN192.

Three example datasets of hue vs. ϕ are shown in Fig. 9. The data were taken at $(u, v) = (100, 300)$, (124, 300), and (136, 300) respectively in the image coordinates depicted in Sect. 5. The ϕ corresponding to the maximum of the curves determines the wall shear stress vector orientation ϕ_τ. The vector-aligned hue value was then converted to the shear stress magnitude via a vector-aligned hue vs. shear stress magnitude calibration curve. The curve fitting procedure was repeated at each pixel within the test area, and all the shear stress vectors over the test surface could be obtained.

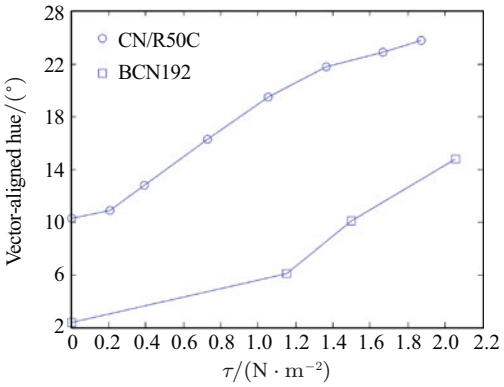

Fig. 8 Vector-aligned hue vs. shear stress magnitude calibration curve (BN/R50C)

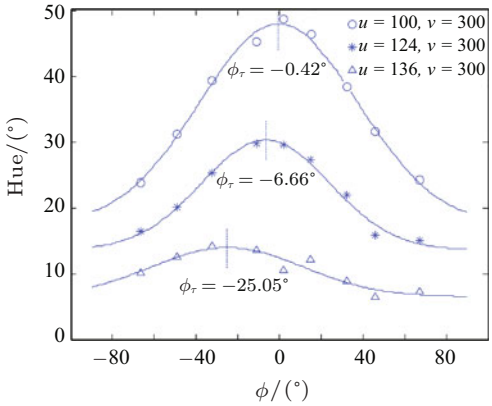

Fig. 9 Hue-ϕ curves for two different shear stress vectors

5 Measurement of surface shear stress vector field beneath a tangential jet

A jet nozzle was affixed to the flat plate, as shown in Fig. 10, to supply dry filtered air at room temperature from a pressurized gas tank connected to a compressor. The jet nozzle was a circular copper tube of outer diameter 12 mm, and inner diameter 3.8 mm, with a blunt tip. A line drawn on the flat plate centerline allowed for an accurate alignment of the jet centerline and the plate centerline. The jet was affixed to the flat plat 1 cm away from the "plug" front edge, and inclined at an angle of about 2.5° relative to the plane of the "plug". A pressure regulator controlled the pressure at a fixed value of 0.09 bars, with a corresponding jet centerline exit velocity of 120 m/s. The regulator was an open-loop controller and thus the jet flow was very unsteady, although care was taken to make sure that the jet flow did not change much during the experiment.

The surface shear stress vector field beneath a tangential jet was measured by Reda et al. [4]. In that work, a special light was used as illumination source, and a new SSLC coating was applied for each view, which made the measurement

complicated and expensive. In the present research, illumination was provided from a simple bulb light, measurements were taken after the coatings produced a steady color and thus only one coating was used for all views required for the Gaussian curve fittings. Three raw images at different in-plane view angles are given in Fig. 11 to demonstrate the color change in BCN/192. The images were rotated into the normal view and the unwanted portions were cropped. The coordinates are in pixel units and the resolution was set so that 1 mm in physical coordinates corresponds to five pixels in the image plane. The image corresponding to $\phi = 2.0°$ is symmetric about the centerline ($u = 100$) due to camera alignment with the plate centerline and the symmetry of the shear vector field itself (magnitudes and directions) relative to the plate centerline. The $\phi = -66.7°$ and $\phi = 67.1°$ images are essentially mirror images, but each appears slightly asymmetric relative to the centerline. This asymmetry is a direct result of the dual dependence of color change response of the coating on shear magnitude and its direction relative to the observer: both quantities vary across the jet-induced shear field.

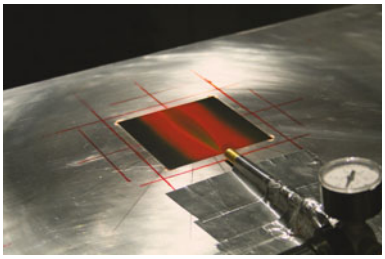

Fig. 10 View of air jet fixed onto the flat plat

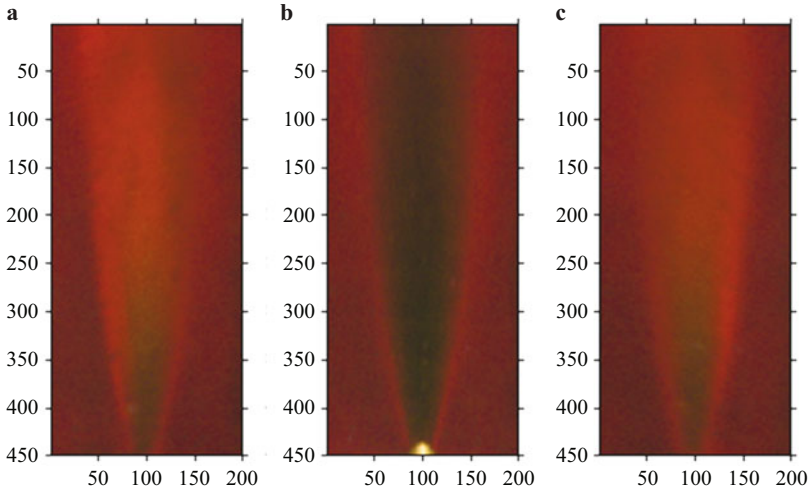

Fig. 11 Liquid crystal coating color change at different in-plane view angles. **a** = –66.7°; **b** = 2.0°; **c** = 67.1°

The curve fitting procedure described in Sect. 4 was repeated at each pixel of the test plate, and all the shear stress vectors over the test surface could be obtained. Unfortunately the color change was not fully calibrated for BCN/192. Figure 12 shows a representation of the wall-jet-induced shear stress vector distribution measured with a BCN/192 coating. The vector field was an average of five measurements. The vectors were computed every four pixels along several profiles. Because only a part of hue vs. shear stress calibration curve was obtained for BCN/192, the vector length was vector-aligned hue but not shear stress magnitude. However, since the relationship between shear stress magnitude and vector-aligned hue is nearly linear, (see Fig. 8), a relative comparison would be possible (e.g., relative to maximum τ, or relative to maximum vector-aligned hue).

In our current research, no attempt was made on the accuracy and uncertainty of SSLC technique. Considerable efforts have been done on this topic by Reda et al. [3–5, 23, 25]. They declared that, in the high shear stress regions,

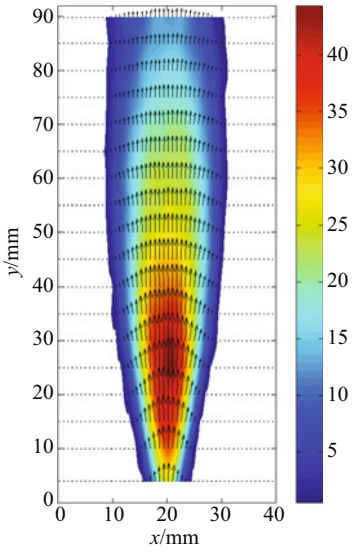

Fig. 12 Surface shear stress field beneath jet flow (color contours of vector-aligned hue)

the standard deviations were in the range of 4% of the local shear magnitude, with corresponding uncertainties of 1°–2° in shear stress orientation; in the low-shear regions, the ability of the SSLC technique to resolve vector orientations, and thus vector magnitudes, was degraded, and the standard deviations of the orientation were as high as 6° with corresponding shear magnitude uncertainties of the order of 10%. However, the accuracy and uncertainty are impacted by many factors, and are different between measurements. Effort should be made on this topic in further research.

6 Measurement of surface shear stress vector field in vortex flow

Vortex generators have long been used in flow control, which delay flow separation and aerodynamic stalling, thereby improving the effectiveness of wings and control surfaces [26]. In this work, we try to measure the surface shear stress vector field in vortex flow using SSLC technique. A delta-wing made of aluminum tape with a height of 1 cm and a base of 2.3 cm was used as a vortex generator. The wing was mounted onto the flat plate with the vertex of the right angle coincident to the plate centerline at a location of 8 cm away from the "plug" leading edge and an offset angle of $\phi = 8°$. An overview of the flat plate with the vortex generator is shown in Fig. 13. The image of each view is rotated into the normal view and the unwanted portions are cut out. Three examples of the coating color change at different views are given in Fig. 14. The resolution was set so that 5 pixels in the image coordinate corresponded 1 mm in the physical coordinate.

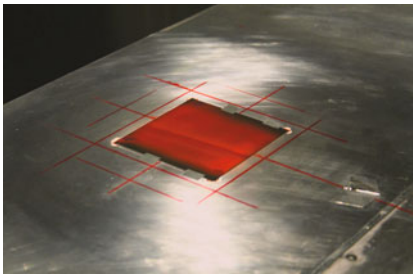

Fig. 13 Overview the flat plate with a vortex generator

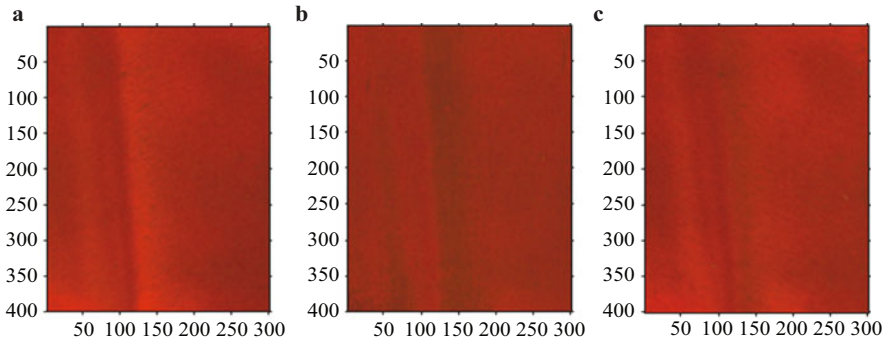

Fig. 14 Liquid crystal color change at different in-plane view angles. **a** = –51.9°; **b** = 1.6°; **c** = 60.9°

Figure 15a shows a three-average surface shear stress vector field downstream of the vortex generator measured by the SSLC technique at a wind tunnel velocity of 19.9 m/s. The vectors were computed every four pixels along several profiles. Because the color change of BCN192 was not fully calibrated, the vector length is vector-aligned hue value rather than shear stress magnitude. The contour was generated based on the vector-aligned hue values. There are

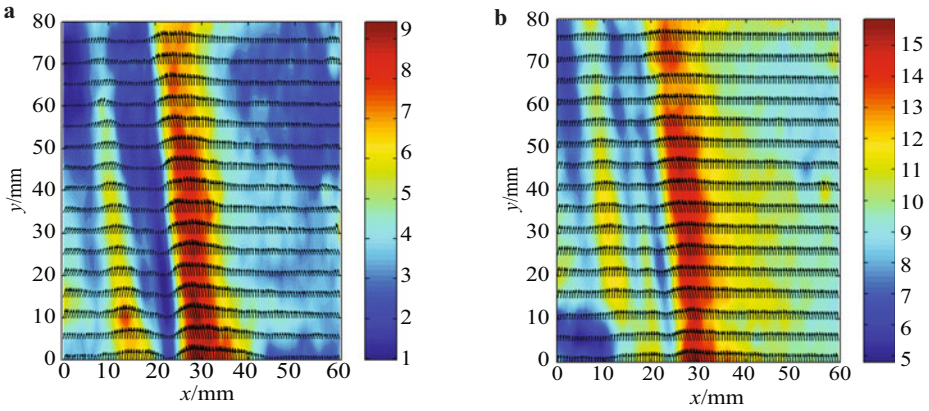

Fig. 15 Surface shear stress field in vortex flow. **a** u = 19.9 m/s; **b** u = 27.4 m/s

two high shear stress areas and two low shear stress areas in Fig. 15a. The higher shear stress area and the low shear stress area next to it are mainly due to the clock-wise vortex primary (see along the flow direction) generated by the delta-wing. The other pair is due to the counter-clockwise induced vortex. For some unknown reasons, there are considerable noises at the low shear stress regions, maybe due to the low sensitivity of liquid crystal coating at this shear stress level, or the gap between the anodized aluminum "plug" and the flat plate. Figure 15b shows a five-average surface shear stress vector field downstream of the vortex generator measured by the SSLC technique at a wind tunnel velocity of 27.4 m/s. The vector field became better at this shear stress level.

7 Measurement of surface shear stress vector field behind a thin cylinder

Surface shear stress field in the junction flow behind a cylinder is very interesting in aerodynamic researches and has been measured using SSLC technique in a two-perspective approach by Fujisawa et al. [6] and Nakano et al. [7]. The current research attempts to measure similar fields based on the technique proposed by Reda et al., which was found more accurate than the two-perspective approach [3]. An overview of the flat plate with cylinder is shown in Fig. 16. The cylinder was fixed onto the anodized aluminum "plug" with the center 34 mm away from the "plug" leading edge. The cylinder has a diameter of 23.6 mm, and a height of 2.6 mm.

Figure 17a shows a five-average surface shear stress vector field behind the cylinder measured by SSLC technique at a wind tunnel velocity of 19.9 m/s. Again, the vector length is vector-aligned hue value rather than shear stress magnitude. The contour is generated based on the vector-aligned hue values. The region around the cylinder was blocked in some views due to cylinder height, and no vector was obtained where less than four views were available, which were the least views for Gauss curve fitting. The blocked views in each curve fit around the cylinder were removed by hand in the curve fitting procedure, because the current program could not tell automatically which views were blocked by the cylinder. The vectors in the high shear stress regions are nice with less noise compared with that obtained by Fujisawa et al. [6]. The vectors in the low shear stress regions are not correct for some unknown reasons, maybe due to the less sensitivity of liquid crystal coating, or the gap between the anodized aluminum "plug" and the flat plate. However, it becomes better in Fig. 17b, which was conducted at a higher velocity of 27.4 m/s. It is noted that there is no reverse flow indicated in Fig. 17. This is because the cylinder used is too thin (2.6 mm in height and 23.6 mm in diameter) to generate reverse flow. The slight reverse flow occurred only at the very neighborhood of the cylinder, and was blocked by the cylinder when recording images. This can be verified from the color change given in Fig. 16. Note that blue (the maximum hue) is observed when the shear stress vector is aligned with, and directed away from the observer (Fig. 11 is an example of this rule).

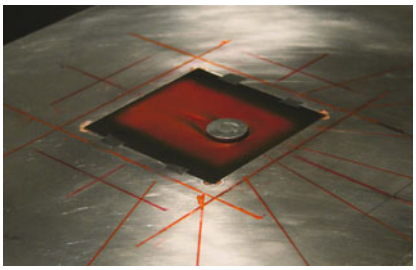

Fig. 16 Overview the flat plate with a cylinder fixed onto the "plug"

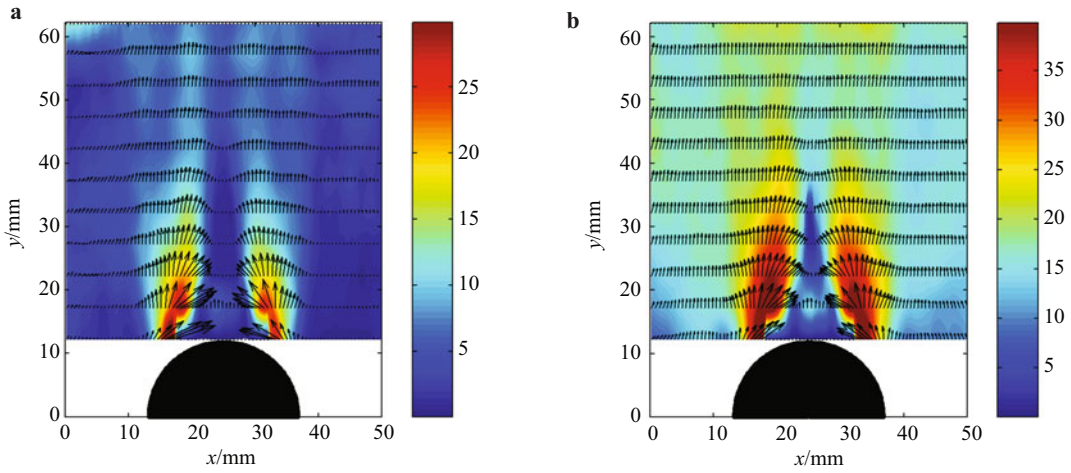

Fig. 17 Surface shear stress fields in cylinder flow. **a** u = 19.9 m/s; **b** u = 27.4 m/s

8 Conclusion

The surface shear stress measurement technique using SSLC was extended to wind tunnel measurements. Only simple and common everyday equipment is used in our experiments; in particular a small tungsten-halogen bulb served as illumination, and a saturation of the SSLC coating color change with time was found. The technique was applied to the measurements of surface shear stress vector distributions in several typical flows, including flow beneath a tangential jet, flow downstream of a vortex generator and flow behind a thin cylinder, although the magnitudes are not fully calibrated. The obtained shear stress vector fields are encouraging. The potential demonstrated in this study warrants further research that will focus on calibrating the vector-aliened hue vs. shear stress magnitude and reducing noise (e.g., using some high-frequency imaging to perform time averaging).

Acknowledgement The authors would like to thank the anonymous reviewers for providing much valuable advice to improve the quality of this paper. The first author would like to express grateful thanks to the Doctorate Creation Foundation of Northwestern Polytechnical University (CX200902).

References

1 Naughton, J. W., Sheplak, M.: Modern developments in shear-stress measurement. Progress in Aerospace Sciences **38**, 515–570 (2002)
2 Haritonidis, J. H.: The measurement of wall shear stress. Advances in Fluid Mechanic Measurements **45**, 229–261 (1989)
3 Reda, D. C., Muratore, J. J. Jr.: A new technique for the measurement of surface shear stress vectors using liquid crystal coatings. AIAA 94-0729 (1994)
4 Reda, D. C., Wilder, M. C., Farina, D. J., et al.: New methodology for the measurement of surface shear-stress vector distributions. AIAA Journal **35**, 608–14 (1997)
5 Reda, D. C., Wilder, M. C., Mehta, R., et al.: Measurement of continuous pressure and shear distributions using coating and imaging techniques. AIAA Journal **36**, 895–859 (1998)
6 Fujisawa, N., Aoyama, A., Kosaka, S.: Measurement of shear-stress distribution over a surface by liquid-crystal coating. Measurement Science and Technology **14**, 1655–1661 (2003)
7 Nakano, T., Fujisawa, N.: Wind tunnel testing of shear-stress measurement by liquid-crystal coating. Journal of Visualization **9**, 135–136 (2006)
8 Fujisawa, N., Oguma, Y., Nakano, T.: Measurements of wall-shear-stress distribution on an NACA0018 airfoil by liquid-crystal coating and near-wall particle image velocimetry (PIV). Measurement Science and Technology **20**, 1–10 (2009)
9 Crafton, J. W., Fonov, S. D., Jones, E. G., et al.: Optical Measurements of Pressure and Shear in a Plasma. AIAA 2005-5006 (2005)
10 Fonov, S. D., Jones, G., Crafton, J., et al.: The development of optical technique for the measurement of pressure and skin friction. Meas. Sci. Technol. **16**, 1–8 (2005)
11 Liu, T., Montefort, J., Woodiga, S., et al.: Global luminescent oil-film skin friction meter. AIAA Journal **46**, 476–485 (2008)
12 Liu, T., Woodiga, S., Ma, T.: Skin friction topology in a region enclosed by penetrable boundary. Exp. Fluids **51**, 1549–1562 (2011)
13 Liu, T., Woodiga, S.: Feasibility of global skin friction diagnostics using temperature sensitive paint. Meas. Sci. Technol. **22**, 1–11 (2011)
14 Zhong, S.: Detection of flow separation and reattachment using shear-sensitive liquid crystals. Exp Fluids **32**, 667–673 (2002)
15 Walsh, E. J., Hernon, D., Davies, M. R. D., et al.: Preliminary measurements from a new flat platefacility for aerodynamic research. In: Proc. of the 6th European Conference On Turbo Machinery, Mar. 7–1, 11 pages. (2005)
16 Sugiyama, H., Minato, R., Mizobata, K., et al.: Study on shock wave and turbulent boundary layer interactions in a square duct at Mach 2 and 4. J. of Thermal. Sci. **15**, 37–42 (2005)
17 Reda, D. C., Wilder, M. C.: Shear-sensitive liquid crystal coating method applied through transparent test surfaces. AIAA Journal **39**, 195–197 (2000)
18 Zhao, J. S., Scholz, P., Gu, L. X.: Color change characteristics of two shear-sensitive liquid crystal mixtures (BCN/192, BN/R50C) and their application in surface shear stress measurements. Chinese Science Bulletin **56**, 2897–2905 (2011)
19 Reda, D. C., Muratore, J. J. Jr., Heineck, J. T.: Time and flow direction responses of shear-stress- sensitive liquid crystal coatings. AIAA Journal **32**, 693–700 (1994)
20 Pascale, D.: RGB Coordinates of the Macbeth Color Checker. The BabelColor Company. (2006)
21 Bonnet, P., Jones, T. V., McDonnell, D. G.: Shear-stress measurement in aerodynamic testing using cholesteric liquid crystals. Liquid Crystals **6**, 271–280 (1989)
22 Mee, D. J., Walton, T. W., Harrison, S. B., et al.: A comparison of liquid crystal techniques for transition detection. AIAA 91-0062 (1991)
23 Reda, D. C., Wilder, M. C., Farina, D. J., et al.: Areal measurements of surface shear stress vector distributions using liquid crystal coatings. AIAA 96-0420 (1996)
24 Hay, J. L., Hollingsworth, D. K.: A comparison of trichromic systems for use in the calibration of polymer-dispersed thermochromic liquid crystals. Exp. Thermal Fluid Sci. **12**, 1–12 (1996)
25 Reda, D. C., Muratore, J. J. Jr.: Measurement of surface shear stress vectors using liquid crystal coatings. AIAA Journal **32**, 1576–1582 (1994)
26 Lin, J. C.: Review of research on low-profile vortex generators to control boundary layer separation. Progress in Aerospace Sciences **38**, 389–420 (2002)